IEEE Access
Multidisciplinary | Rapid Review | Open Access Journal

Received February 10, 2020, accepted March 10, 2020, date of publication March 20, 2020, date of current version April 8, 2020.

Digital Object Identifier 10.1109/ACCESS.2020.2982277

A Multi-View Discriminant Learning Approach for Indoor Localization Using Amplitude and Phase Features of CSI

TAHSINA FARAH SANAM, (Student Member, IEEE), AND HANA GODRICH, (Senior Member, IEEE)
Department of Electrical and Computer Engineering, Rutgers University, Piscataway, NJ 08854, USA
Corresponding author: Tahsina Farah Sanam (tahsina.farah@rutgers.edu)

ABSTRACT Location Based Service (LBS) is one of the important aspects of a smart city. Accurate indoor localization plays a vital role in LBS. The ability to localize various subjects in the area of interest facilitates further ubiquitous environments. Specifically, device free localization using wireless signals is getting increased attention as human location is estimated using its impact on the surrounding wireless signals without any active device tagged with subject. In this paper, we propose MuDLoc, the first multi-view discriminant learning approach for device free indoor localization using both amplitude and phase features of Channel State Information (CSI) from multiple Access Points (APs). The same location oriented CSI data can be observed by different APs, thus generating multiple distinct even heterogeneous samples. Multi-view learning is an emerging technique in machine learning which improve performance by utilizing diversity from different view data. In MuDLoc, the localization is modeled as a pattern matching problem, where the target location is predicted based on similarity measure of CSI features of an unknown location with those of the training locations. MuDLoc implements Generalized Inter-view and Intra-view Discriminant Correlation Analysis (GI^{2}DCA), a discriminative feature extraction approach that incorporates inter-view and intra-view class associations while maximizing pairwise correlations across multi-view data sets. Experimental results from two cluttered environments show that MuDLoc can estimate location with high accuracy which outperforms other benchmark approaches.

INDEX TERMS Indoor localization, device free, multi-view discriminant learning, amplitude and phase features, CSI.

I. INTRODUCTION

Learning important human contextual information is one of the fundamental features to establishing a smart environment. The ability to localize various subjects indoor can potentially support a broad array of applications including elder care, rescue operations, vehicle parking management, building occupancy statistics, security enforcement, etc. Unlike outdoor localization that can rely on the use of Global Positioning System (GPS), that is based on transmission of Line-of-Sight (LOS) paths, indoor localization suffers from a lot of challenges due to indoor radio propagation, such as multipath, fading, shadowing, etc. [1], [2]. Wireless signals, specifically Wi-Fi signals have emerged as one of the most pervasive signals for this application. Human presence is interfering with these signals. By observing the channel features over time, people's location can be inferred by comparing them against pre-constructed signal profiles, which is commonly known as fingerprinting approach [3], [4]. In most of the fingerprinting-based approaches, coarse-grained Received Signal Strength (RSS) are used as the wireless signatures for localization [5]–[9]. RSS varies over distance on the order of the signal wavelength and fluctuates over time, which degrades localization performance with lower accuracy [3]. In order to overcome the limitations of RSS, recently different applications are widely using the fine grained PHY layer CSI [10], [11]. Leveraging off-the-shelf commodity devices, CSI is available in several Wi-Fi network interface cards (NIC), such as Intel 5300 NIC [12], [13]. In IEEE 802.11n communication, CSIs can be obtained from Multiple Input Multiple Output (MIMO) Orthogonal frequency Division Multiplexing (OFDM) systems. Unlike RSS, each CSI measurement provides us with amplitude and phase information for subcarrier level channels for each antenna link. These fine

The associate editor coordinating the review of this manuscript and approving it for publication was Mu-Yen Chen.

grained CSI is not only richer in multipath information, but also more stable than RSS for a given location. Therefore, CSI is considered as a preferable choice of wireless signature to realize an improved indoor localization system [14]–[20].

There exists a rich body of previous work in the field of device based indoor localization, where the target is required to carry special devices, like WiFi-enabled smartphones or RFID tags, etc. [14]–[16]. However, with the growth of LBS, recently device free localization is drawing significant interest to meet some emerging application demands [8], [19], [21]. In device free localization, a transceiver free target can be localized by utilizing the feature pattern of the wireless signal that is being interfered by the presence of the subject. To this end, a pattern matching approach of device free indoor localization has emerged as an effective technique, where CSI features of the unknown location is matched with those of the training locations in order to predict the location.

Indoor localization with device free approach has been explored in various methods [8], [9], [19], [20], [22]–[24]. These methods consider either RSS value of wireless signals or only the amplitude of CSI. In [8], localization is performed using probabilistic classification approaches that are based on discriminant analysis of wireless sensor-based RSS value. Another RSS based localization is proposed in [9], where an adaptive spring relaxation approach is exploited for localization. However, dependence upon the coarse RSS measurements limits the performance of the above methods. Indoor localization using CSI has been explored in [19], [20]. In [19], authors perform CSI based device free localization through a probabilistic approach and showed improvement in localization with 85% accuracy where [20] adopts a power fading model-based localization and achieves 90% accuracy with 1.5 meter localization error. Both methods considered only the amplitude values of CSI from a single AP, as such, lots of useful information embedded with the phase is not used. Moreover, all these methods consider CSI measurements either from a single AP or perform the localization task by averaging CSI measurements from multiple APs. However, a set of CSI measurements, simultaneously recorded from multiple APs for a particular target location should share some common features, which might be correlated. Some useful information, involved with multiple OFDM channel correlations, may lost if measurements from each AP are considered independently. As a result, ignoring phase information from CSI measurements as well as separate utilization of CSI measurements from multiple APs limit the performance of existing state-of-the-art approaches in achieving higher accuracy for localization.

In this paper, MuDLoc, a multi-view discriminant learning approach for device free indoor localization using CSI is proposed. In MuDLoc, the localization problem is formulated as a cell classification problem, where the area is virtually partitioned into some uniform square grid cells, which are considered as class. Under this setting, MuDLoc uses CSI fingerprints to classify a testing entity with an unknown cell ID/class label. However, this method utilizes CSI measurements recorded from multiple APs for a particular target location in order to extract common features shared by all APs. In this case, CSI measurements obtained from each AP can be referred to as a particular view and sets of CSI measurements, simultaneously recorded from multiple APs for a particular target location can be considered as multi-view data. For classification problems under multi-view setting, both inter-view and intra-view class separations are important issues to consider, where samples in one class from multiple views should be close to each other (intra-view), while samples in different classes from multiple views should be far away from each other (inter-view). However, direct matching of the data samples across various feature spaces is infeasible. Subspace learning offers an effective approach to solving the problem, which learn a common feature space from multi-view spaces. Therefore, MuDLoc exploits a multi-view learning approach to extract joint spatial features from multi-view CSI data, that are recorded from multiple APs.

Various multi-data processing techniques have been reported in literature. The work in [25] proposes semi-supervised multi-view correlation feature learning (SMCFL), for webpage classification. In addition to maximizing the correlation between intra-class samples, and the correlation between inter-class samples, this work maximizes the global correlation among both labeled and unlabeled samples. In [26], another approach for semi supervised multi-view feature learning for webpage classification is proposed, which jointly learns multiple view-individual transformations and one sharable transformation to explore the view-specific property for each view and the common property across views. A multi-view dictionary learning technique (MDVSD) is proposed in [27], which learns a structured dictionary shared by all views and multiple view-specific structured dictionaries with each corresponding to a specific view. MDVSD makes the view-specific dictionaries corresponding to different views uncorrelated for effectively exploring the diversity of different views. Canonical Correlation Analysis (CCA) is one of the multi-data processing methods that deals with linear relationship between two or more multi-dimensional variables [28], [29]. Multi-view CCA (MCCA) was developed as an extension of CCA to find multiple linear transforms that maximize overall correlation among canonical variates from multiple sets of random variables [30]–[32]. However, MCCA does not take discriminant information into account, which may degrade classification performance across classes. The supervised information was incorporated in a generalized multiview analysis framework (GMA), leading to a discriminant common subspace [33]. However only the intra-view discriminant information was considered in GMA, ignoring inter-view discriminant information, which may degenerate performance of cross-view matching. The work in [34] addressed the intra-view and inter-view supervised correlation analysis method by studying the CCA based multi-view feature learning technique. However, in CCA based multi-view subspace learning methods, learned

features are dedicated to depicting only intrinsic correlation among multiple views. Another approach of multi-view learning is discriminant analysis based multi-view subspace learning method which aims to achieve multiple linear transformations, which maximizes the between-class variations of low-dimensional embeddings and minimizes the within-class variations of low-dimensional embeddings. Therefore, in order to exploit class structures for cross-view recognition, the proposed MuDLoc method implements Generalized Inter-view and Intra-view Discriminant Correlation Analysis (GI^{2}DCA), which, unlike [34], utilizes the principles of both CCA and discriminant analysis based multi-view subspace learning methods to take advantage of these two algorithms. GI^{2}DCA is a subspace learning approach that can learn single unified discriminant common space from the joint spatial filtering of multiple sets of CSI data recorded for a particular target location. In this common space, the between-class variations from both inter-view and intra-view are maximized, while keeping the projections of different views close to each other in the latent common space. Therefore, unlike MCCA and GMA, both inter-view and intra-view class structures are preserved in GI^{2}DCA, which helps to improve the localization performance through cell classification approach.

Finally, MuDLoc system exploits both the amplitude and the phase information of multi-view CSI data to learn the discriminative common space. In 5 GHz Intel 5300 NIC, the phase difference between two receiver antennas is relatively more stable than the raw CSI phase [35]–[37]. Therefore, in addition to amplitude information, the proposed method utilizes CSI phase difference information between adjacent receiver antennas for consecutive packets under the multi-view setting. By utilizing both the amplitude and the phase difference between receiver antennas as location features, complete wireless propagation features can be exploited for better localization. Once the discriminant features are obtained with GI^{2}DCA analysis, MuDLoc performs the localization through a pattern matching approach. To achieve this goal, an euclidean distance-based similarity measure approach is utilized, where it finds the best cell match to localize a test subject. The whole system is designed to localize single target in the area of interest. Multi target localization involves different challenges and is left for future research. The main contributions of the paper can be summarized as follows.

1) Utilizing CSI measurements from multiple APs through the multi-view learning approach using GI^{2}DCA, where both inter-view and intra-view class structures are preserved. Since localization problem is formulated as a cell classification approach, incorporating inter-view and intra-view class structures in multi-view analysis facilitates to achieve significant improvement in localization accuracy.
2) The MuDLoc system leverages both the amplitude and phase difference of adjacent antennas in a MIMO OFDM system, and thereby complete wireless propagation features are utilized in order to achieve higher localization accuracy.
3) Extensive experimentation performed in two cluttered indoor environments are used to verify the effectiveness of MuDLoc, demonstrating it outperforms previously proposed state-of-the-art localization methods.

The rest of the paper is structured as follows. Section II presents the motivation behind the proposed MuDLoc system. Preliminaries on CSI, phase information and basic multi-data processing using CCA are described in Section III. The MuDLoc method, a multi-view discriminant learning approach for indoor localization, is introduced in Section IV. Section V describes the system experimental setup and evaluates the performance of the proposed method. Finally, concluding remarks are discussed in Section VI.

II. MOTIVATION

In the proposed MuDLoc sytem, the area is considered as a grid of small square cells. MuDLoc aims to use CSI fingerprints collected at Detecting Point (DP) from multiple APs in order to classify a testing entity with an unknown cell ID.

The motivation for utilizing multi-view learning of CSI measurements stems from the idea that, people can see a location from different views. Similarly, CSI data for a particular location can be observed at different viewpoints or by different APs, thus generating multiple distinct even heterogeneous samples. In this case, we refer each variable group to as a particular view and these CSI measurements from multiple APs are known as multi-view data. These multi-view CSI measurements should share some common features for a particular target location, which might be correlated. Some useful information, involved with multiple OFDM channel correlations, may lost if measurements from each AP are considered independently. Therefore, joint learning of multiple view-specific linear transforms facilitates to obtain a discriminant common space for robust location estimation from multiple views in contrast to that of a single view (AP) based localization approach. Motivated by this idea, MuDLoc exploits CSI measurements recorded from multiple APs through joint spatial filtering in order to utilize a multi-view learning approach for better localization performance. Utilizing CSIs from multiple APs also helps to improve localization accuracy in indoor environment. Multi-view CSI data reflect different characteristics of the multipath patterns, affected by the presence of a subject at a particular location. However, these CSI measurements of different APs are not affected equally by indoor multipath. In a cluttered indoor environment, CSIs from one AP may be affected badly due to multipath effect while that from other APs may not. If CSIs of one AP is blocked, CSIs from other APs might compensate for that and thereby help to mitigate the multipath effect to a great extent.

The motivation for utilizing different modalities of CSI measurements in term of amplitude and phase stems from the idea that, under some indoor scenarios, amplitude and phase are usually complementary to each other. When a signal is

blocked, the average amplitude will be significantly reduced, but the phase difference between two receiver antennas will be less affected. The opposite effect is obtained when the the line of sight (LOS) components are weaker than the non line of sight (NLOS) components. In such a scenario, the average amplitude are more likely to help to improve the localization accuracy than the phase difference data. Therefore, MuDLoc aims to utilize both the amplitude and the phase of CSI for obtaining better localization performance.

To validate the proposed idea, we carry out some preliminary tests. We transform the CSI measurements from multiple OFDM channels of each AP-DP link into a feature matrix corresponding to an image. Since the OFDM channels are correlated, for each AP-DP link, CSI measurements received from multiple antenna channels are also correlated. Therefore, instead of dealing the CSI measurements from each antenna channel independently, joint utilization of CSI measurements from all the antenna channels offers us to leverage channel correlations for improved localization. This motivates us to transform the CSI measurements of sub carriers from multiple transmission-receiver antenna channels of each AP-DP link into a feature matrix corresponding to the pixel value of an image. Therefore, from the two-dimensional perspective, each column (x-axis) corresponds to a packet sample and for each sample, and the CSIs in the rows (y-axis) correspond to subcarriers from all channels for one AP. Fig. 1 and 2 illustrates some CSI amplitude and phase feature images, respectively; obtained from multiple APs while a person is located at different locations. From the figures, it can be seen that the CSI amplitude and phase feature images from different locations have different patterns. In addition, for both the amplitude and phase, features corresponding to the same cell/location are different for two different APs. Therefore, CSI amplitude and phase feature images that are collected from different APs can be considered as good candidates for designing a robust localization system through multi-view learning approach.

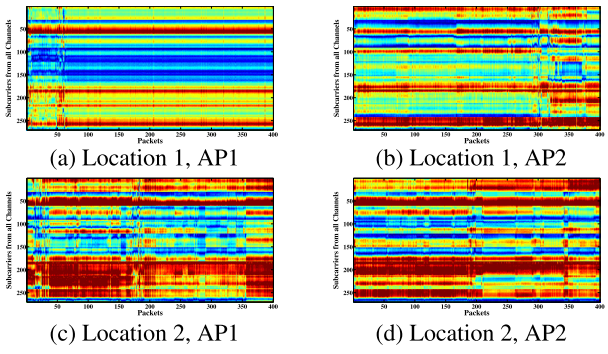

(a) Location 1, AP1 (b) Location 1, AP2

(c) Location 2, AP1 (d) Location 2, AP2

FIGURE 1. Feature images of different locations using CSI amplitude.

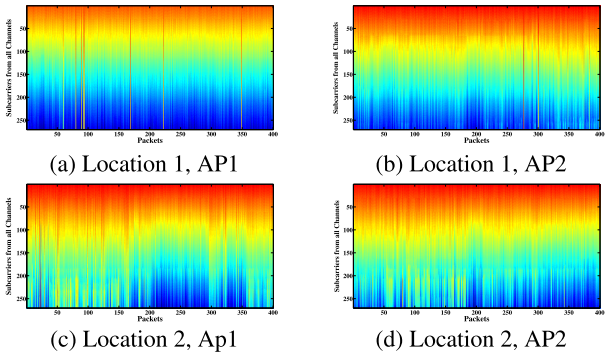

(a) Location 1, AP1 (b) Location 1, AP2

(c) Location 2, Ap1 (d) Location 2, AP2

FIGURE 2. Feature images of different locations using CSI phase.

III. PRELIMINARIES

A. CHANNEL STATE INFORMATION

The wireless channel in MIMO-OFDM technology is partitioned into orthogonal subcarriers. Each of these subcarriers represents a narrow-band flat fading channel. In the frequency domain, these narrow-band flat fading channel is modeled as,

$$y = \mathscr{H}x + \zeta, \tag{1}$$

where y and x are the received and the transmitted signal vectors respectively, ζ is the noise vector and $\mathscr{H}$ denotes the channel matrix. The channel matrix $\mathscr{H}$ can be estimated by,

$$\hat{\boldsymbol{H}} = \frac{y}{x}, \tag{2}$$

where $\hat{\boldsymbol{H}}$ represents the PHY layer CSIs over multiple subcarriers. For one transmitter-receiver (Tx-RX) antenna pair, $\hat{\boldsymbol{H}}$ is a $S \times N$ matrix for each AP-DP link, where S denotes the number of subcarriers for each antenna pair and N is the number of measurements. CSI of a single subcarrier k is a complex value [38],

$$h_k = R_k + jI_k = |h_k|e^{jsin\theta_k}, \tag{3}$$

where R_k and I_k are the in-phase and quadrature components, respectively; $|h_k|$ is the amplitude, and θ_k is the phase of k-th subcarrier. The amplitude response of subcarrier k is $|h_k| = \sqrt{R_k^2 + I_k^2}$, and the phase response is computed by $\angle h_k = \arctan(I_k/R_k)$. We group CSIs of all Tx-Rx antenna pairs of each AP-DP link as,

$$\boldsymbol{H} = [\hat{\boldsymbol{H}}_1; \hat{\boldsymbol{H}}_2; \ldots; \hat{\boldsymbol{H}}_l], \tag{4}$$

where l denotes the Tx-Rx antenna pair index for each AP-DP link and $\boldsymbol{H} \in \mathbb{R}^{d \times N}$, where $d = S \times l$, the total number of subcarriers from all Tx-Rx antenna pairs. We can consider $\boldsymbol{H}$ as the feature image of CSI, where each column corresponds to an image sample and for each sample, the CSIs in the rows corresponds to the pixel values of an image.

B. CSI PHASE INFORMATION

Although off-the-shelf commodity device, such as Intel 5300 NIC, provides us with CSI phase information, this phase is highly random. The performance of indoor localization degrades with high localization error if the raw phase data is directly used. The randomness in the phase stems from hardware imperfection of the commodity device, specifically from

the lack of time and frequency synchronization of the transmitter and receiver. Therefore, state-of-the-art research works utilize only the amplitude information of CSI and ignore the phase information. Consequently, some useful information, involved with phase, may lost if the phase information is discarded. In order to utilize CSI phase, phase sanitization can be done by linear transformation of the phase values or by utilizing the phase difference between two antennas in 2.4 GHz band [39], [40]. Although CSI phase can be stabilized with the above methods, the average phase value obtained from these methods becomes different from the actual phase of the measured CSI due to the firmware problem in the 2.4 GHz band [36]. In order to avoid the problem of random phase error, we exploit the difference in phase values between two receiver antennas in 5GHz band. In [35], we showed that in 5GHz 5300 NICs, the phase difference between two receiver antennas becomes highly stable for consecutively received data packets. Based on the work in [35], here we utilize the phase difference information instead of raw phase. Let, θ_k denotes the phase of measured CSI from any subcarrier k of one AP. According to [41], [42], θ_k can be expressed as,

$$\theta_k = \phi_k + k(\delta_{PB} + \delta_{SF}) + \delta_{CF}, \tag{5}$$

where ϕ_k is the original phase of subcarrier k caused by the channel propagation, δ_{PB}, δ_{SF}, and δ_{CF} represents phase errors arising from the packet boundary detection (PBD), the sampling frequency offset (SFO), and central frequency offset (CFO), respectively. Our aim is to eliminate the impact of error parameters δ_{PB}, δ_{SF}, and δ_{CF} from the measured phase value θ_k in order to avoid the effect of random phase error on localization.

Generally, the time shift parameter τ_{PB} from the packet boundary detection give rise to the phase error uncertainty δ_{PB}. On the other hand, δ_{SF} is caused by the offset of the sampling frequencies of the sender and the receiver. In addition, the phase error δ_{CF} is generated from the incomplete central frequency offset compensation due to hardware imperfection of the transmitter and receiver. In [35], it has been shown that all of these error parameters of CSI phase depend upon a number of OFDM system parameters, such as, packet boundary detection delay, sampling periods of the receiver and the transmitter, current packet sampling time offset, difference of center frequency between the transmitter and receiver, etc. Since off-the-shelf devices provide us with only physical layer CSI data, some of the parameters are unknown. In addition, some of these parameters varies for different packets which in turn causes variation in δ_{PB}, δ_{SF}, and δ_{CF} over time [42]. Hence, the original phase cannot be properly detected by the measured CSI phase.

However, the receiver antennas of a particular NIC have the same clock and same down-converter frequency. As a result, for a particular subcarrier k, the measured CSI phase will also have the same central frequency difference, same delay in packet detection and same sampling period. The difference in measured CSI phase between two receiver antennas at subcarrier k becomes stable can be approximated as,

$$\Delta\theta_k \approx \Delta\phi_k, \tag{6}$$

where $\Delta\phi_k$ is the phase difference of original phase between two adjacent antennas on subcarrier k. From (6) it can be seen that the effect of random phase errors are minimized since the random terms associated with δ_{PB}, δ_{SF}, and δ_{CF} are eliminated. The phase differences are further shifted to be zero mean in order to ensure that initial phase offset errors for each packet are also minimized. Consequently, over different packets, $\Delta\theta_k$ becomes more stable compared to the individual CSI phase value.

C. CANONICAL CORRELATION ANALYSIS

For multi-data processing, Canonical Correlation Analysis (CCA) is considered as one of the useful tools for finding a linear relationship between two feature sets [28]. CCA finds a common space for two views such that the correlation between these transformed feature sets are maximized in the common subspace.

Suppose that n training feature vectors of the data from two different views are denoted by two matrices, $\boldsymbol{X}_1 \in \mathbb{R}^{p\times n}$ and $\boldsymbol{X}_2 \in \mathbb{R}^{q\times n}$, with dimension p and q for each training vector, respectively. For simplicity, we assume that the observed samples are mean-centered. CCA aims to find a common subspace such that the pair-wise correlation across the two feature sets are maximized. In order to project the samples from two views into the common subspace respectively, two linear transforms $\boldsymbol{w}_1$ and $\boldsymbol{w}_2$ are obtained by maximizing the correlation between $\boldsymbol{w}_1^T\boldsymbol{X}_1$ and $\boldsymbol{w}_2^T\boldsymbol{X}_2$ as below [28], [43]:

$$\begin{aligned} &\max_{\boldsymbol{w}_1,\boldsymbol{w}_2} \boldsymbol{w}_1^T\boldsymbol{X}_1\boldsymbol{X}_2^T\boldsymbol{w}_2 \\ &\text{subject to } \boldsymbol{w}_1^T\boldsymbol{X}_1\boldsymbol{X}_1^T\boldsymbol{w}_1 = 1, \quad \boldsymbol{w}_2^T\boldsymbol{X}_2\boldsymbol{X}_2^T\boldsymbol{w}_2 = 1. \end{aligned} \tag{7}$$

Applying Lagrange multiplier on (7), the optimization problem of CCA can be solved by a generalized eigenvalue problem as follows [30]:

$$\begin{bmatrix} \boldsymbol{0} & \boldsymbol{X}_1\boldsymbol{X}_2^T \\ \boldsymbol{X}_2\boldsymbol{X}_1^T & \boldsymbol{0} \end{bmatrix} \begin{bmatrix} \boldsymbol{w}_1 \\ \boldsymbol{w}_2 \end{bmatrix} = \lambda \begin{bmatrix} \boldsymbol{X}_1\boldsymbol{X}_1^T & \boldsymbol{0} \\ \boldsymbol{0} & \boldsymbol{X}_2\boldsymbol{X}_2^T \end{bmatrix} \begin{bmatrix} \boldsymbol{w}_1 \\ \boldsymbol{w}_2 \end{bmatrix}, \tag{8}$$

where the degree of correlation between projections are reflected by the generalized eigenvalue λ.

The CCA based approach described above is unsupervised. For pattern recognition problems, separating the classes is an important issue to consider. In CCA, the features are decorrelated, but the concept of class structure among the samples are not considered. In order to exploit class structures, discriminant CCA (DCCA) is proposed which takes into consideration both within-class and between-class correlation in CCA [44]. DCCA preserves the class structures for C classes between two views through the following optimization problem:

$$\begin{aligned} &\max_{\boldsymbol{w}_1,\boldsymbol{w}_2} \boldsymbol{w}_1^T\boldsymbol{X}_1\boldsymbol{G}\boldsymbol{X}_2^T\boldsymbol{w}_2 \\ &\text{subject to } \boldsymbol{w}_1^T\boldsymbol{X}_1\boldsymbol{X}_1^T\boldsymbol{w}_1 = 1, \quad \boldsymbol{w}_2^T\boldsymbol{X}_2\boldsymbol{X}_2^T\boldsymbol{w}_2 = 1. \end{aligned} \tag{9}$$

where

$$\boldsymbol{G} = \begin{bmatrix} \boldsymbol{I}_{n_1 \times n1} & & & \boldsymbol{0} \\ & \ddots & & \\ & & \boldsymbol{I}_{n_c \times n_c} & \\ \boldsymbol{0} & & & \ddots \\ & & & \boldsymbol{I}_{n_C \times n_C} \end{bmatrix}. \quad (10)$$

Applying Lagrange multiplier on (9), the optimization problem of DCCA can be solved by a generalized eigenvalue problem as follows [44]:

$$\begin{bmatrix} \boldsymbol{0} & \boldsymbol{X}_1\boldsymbol{G}\boldsymbol{X}_2^T \\ \boldsymbol{X}_2\boldsymbol{G}\boldsymbol{X}_1^T & \boldsymbol{0} \end{bmatrix} \begin{bmatrix} \boldsymbol{w}_1 \\ \boldsymbol{w}_2 \end{bmatrix} = \lambda \boldsymbol{B} \begin{bmatrix} \boldsymbol{w}_1 \\ \boldsymbol{w}_2 \end{bmatrix}. \quad (11)$$

where,

$$\boldsymbol{B} = \begin{bmatrix} \boldsymbol{X}_1\boldsymbol{X}_1^T & \boldsymbol{0} \\ \boldsymbol{0} & \boldsymbol{X}_2\boldsymbol{X}_2^T \end{bmatrix}. \quad (12)$$

IV. THE MuDLoc SYSTEM

In MuDLoc the overall localization is performed through an offline phase and an online phase as described below.

A. OFFLINE PHASE

1) CONSTRUCTION OF CSI AMPLITUDE AND PHASE FEATURE IMAGE

Exploiting both amplitude and the phase features of CSI from commodity WiFi device facilitates to utilize complete multipath features to achieve a high precision indoor localization system. In MuDLoc, the area is considered as a grid of small square cells. Let, there are C cells and M APs in that area of interest. In the offline stage, a set of CSI measurements are collected with the subject present in a cell, c, where c = 1,2,…,C. Each cell can be considered as a class. Let class c has n_c data samples. Next, CSI feature image $\boldsymbol{H}_i^c$ is generated for each cell using (4), where i = 1,2,…,M. $\boldsymbol{H}_i^c$ represents the effect of the presence of an entity on the i-th AP's CSI for the entity located at a particular position or cell, c. From $\boldsymbol{H}_i^c$, CSI amplitudes are extracted to generate amplitude feature image, $\boldsymbol{X}_i$ of size $d_{X_i} \times n$, where $n = \sum_{j=1}^{C} n_c$. Similarly, the phase information is also extracted from $\boldsymbol{H}_i^c$ in order to generate CSI phase based feature image for each cell and then phase feature image, $\boldsymbol{Y}_i$ of size $d_{X_i} \times n$ is generated based upon the CSI phase difference of two adjacent receiver antennas for each AP using (6). These phase differences on a particular subcarrier between two receiver antennas in MIMO OFDM system are relatively stable compared to the raw phase information, since the effect of random phase errors are minimized as described in section III-B.

Once both the amplitude and phase features of CSI in terms of amplitude and the phase difference-based feature images for all the APs in the area of interest are obtained, the system then exploits multi-view discriminant learning approach in order to obtain a discriminant common spaces for localization.

2) MULTI-VIEW DISCRIMINANT LEARNING OF CSI

Good performance of the CCA-based indoor localization has been confirmed by the study on amplitude-based CSIs [21]. However, in [21] only the CSI amplitude from a single AP (view) has been considered for location estimation. We consider that some common features should be shared by a set of CSI measurements recorded from multiple APs for a particular target cell. Motivated by the CCA based discriminant learning of CSI for indoor localization, in this section we propose multi-view discriminant learning of CSI to achieve better localization performance. The optimal amplitude and phase feature sets of CSIs are first learned from the joint spatial filtering of multiple sets of CSI amplitude and phase feature images, respectively; and are subsequently used in the feature fusion [45], where the transformed amplitude and phase feature images are stacked to obtain the complete feature set for cell recognition.

CCA based approach, described in section III-C is only designed for two-view case, and thus the pairwise strategy is needed when applied to the multi-view scenario. However, generalization of the CCA to multiple sets has to be equivalent to the case of two set CCA. MCCA is a generalization of CCA to more than two views of data, where the overall correlation among canonical variates from multiple sets of random variables is maximized through the optimization of the objective function of correlation matrix of the canonical variates [30]–[32]. The five most discussed versions of MCCA are: (1) SUMCOR, maximize the sum of all entries in the correlation matrix; (2) MAXVAR, maximize the largest eigenvalue of the correlation matrix; (3) SSQCOR, maximize the sum of squares of all entries in the correlation matrix; (4) MINVAR, minimize the smallest eigenvalue of the correlation matrix; (5) GENVAR, minimize the determinant of the correlation matrix. Similar results are obtained for all of the five objective functions on a group dataset [46], [47]. This paper summarizes the classical sum of correlations generalization (SUMCOR) and MCCA is used as an abbreviation for SUMCOR maximization approach throughout the paper. [30], [31].

Let, for M APs, multiple sets of random variables with n samples of d_i dimension are denoted by $\boldsymbol{X}_i \in \mathbb{R}^{d_i \times n}$, where, i = 1, 2, …, M. We assume that $\boldsymbol{X}_i$'s are normalized to have zero mean and unit variance. MCCA aims to find a set of linear transforms $\boldsymbol{w}_i\big|_{i=1}^{M}$, to respectively project the samples of M views $\{\boldsymbol{X}_1, ..., \boldsymbol{X}_M\}$ to one common space, i.e., $\{\boldsymbol{w}_1^T\boldsymbol{X}_1, \ldots, \boldsymbol{w}_M^T\boldsymbol{X}_M\}$. The total correlation in the common space is maximized as below:

$$\max_{\boldsymbol{w}_1,\ldots,\boldsymbol{w}_N} \rho = \sum_{\substack{i,j=1 \\ i \neq j}}^{M} \boldsymbol{w}_i^T \boldsymbol{X}_i \boldsymbol{X}_j^T \boldsymbol{w}_j$$
$$\text{s.t. } \boldsymbol{w}_i^T \boldsymbol{X}_i \boldsymbol{X}_i^T \boldsymbol{w}_i = 1, \quad i = 1, 2, \ldots, M \quad (13)$$

where $\boldsymbol{w}_i$ are the unknown transforms that have to be estimated for each matrix $\boldsymbol{X}_i$, which are M known full-rank data matrices. The full-rank constraint of data matrices may

be relaxed by regularizing the estimated covariance matrices [48]. We can rewrite Eq. (13) as,

$$\max_{\boldsymbol{w}} \rho = \boldsymbol{w}^T(\boldsymbol{C} - \boldsymbol{D})\boldsymbol{w}$$
$$\text{s.t. } \boldsymbol{w}^T\boldsymbol{D}\boldsymbol{w} = 1, \tag{14}$$

where,

$$\boldsymbol{C} = \begin{bmatrix} \boldsymbol{X}_1\boldsymbol{X}_1^T & \dots & \boldsymbol{X}_1\boldsymbol{X}_M^T \\ \vdots & \ddots & \vdots \\ \boldsymbol{X}_M\boldsymbol{X}_1^T & \dots & \boldsymbol{X}_M\boldsymbol{X}_M^T \end{bmatrix}, \tag{15}$$

$$\boldsymbol{D} = \begin{bmatrix} \boldsymbol{X}_1\boldsymbol{X}_1^T & \dots & \boldsymbol{0} \\ \vdots & \ddots & \vdots \\ \boldsymbol{0} & \dots & \boldsymbol{X}_M\boldsymbol{X}_M^T \end{bmatrix}, \tag{16}$$

$$\boldsymbol{w} = \begin{bmatrix} \boldsymbol{w}_1 \\ \vdots \\ \boldsymbol{w}_M \end{bmatrix}. \tag{17}$$

Applying Lagrange multiplier on (14), the optimization problem of MCCA can be solved by a generalized eigenvalue problem. Using the Lagrange multiplier λ, the cost function J is formed as below, and the unknown transforms $\boldsymbol{w}$ is found to maximize it:

$$J = \boldsymbol{w}^T(\boldsymbol{C} - \boldsymbol{D})\boldsymbol{w} + \lambda(\boldsymbol{w}^T\boldsymbol{D}\boldsymbol{w} - 1). \tag{18}$$

Taking the derivative with respect to $\boldsymbol{w}$, one can write,

$$(\boldsymbol{C} - \boldsymbol{D})\boldsymbol{w} = \lambda\boldsymbol{D}\boldsymbol{w}. \tag{19}$$

Eq. (19) represents a general eigenvalue decomposition problem and the largest eigenvector maximizes the cost function in Eq. (18). Therefore, the eigenvector corresponding to the largest eigenvalue in the general eigen decomposition of Eq. (19) provides the solution for the optimization problem of MCCA. The λ in Eq. (19) can be obtained by left multiplication with $\boldsymbol{w}^T$, which, applying the constraint from Eq. (14), implies $\lambda = \rho$. Similar to CCA, the number of samples in each view for MCCA should be the same. In addition, MCCA is an unsupervised method. MCCA only obtain a common space by maximizing the correlation between multiple views, neither intra-view correlation nor label information is considered. In order to obtain discriminative common subspace for all views, GMA in [33] proposed a general framework for multiview analysis, where the supervised structure of each view is preserved while keeping the projections of different views in the latent common space close to each other as follows:

$$\max_{\boldsymbol{w}_1,\dots,\boldsymbol{w}_N} \sum_{i=1}^{M} \alpha_i \boldsymbol{w}_i^T \boldsymbol{S}_i \boldsymbol{w}_i + \sum_{\substack{i,j=1 \\ i\neq j}}^{M} \beta_{i,j} \boldsymbol{w}_i^T \boldsymbol{X}_i \boldsymbol{X}_j^T \boldsymbol{w}_j$$
$$\text{s.t. } \sum_{i}^{M} \gamma_i \boldsymbol{w}_i^T \boldsymbol{X}_i \boldsymbol{X}_i^T \boldsymbol{w}_i = 1, \tag{20}$$

where α_i, $\beta_{i,j}$ and γ_i are the balance parameters; and $\boldsymbol{S_i}$ is the between-class scatter matrix for the i-th view, which is defined as:

$$\boldsymbol{S_i} = \sum_{c=1}^{C} n_c^i (\mu_c^i - \mu^i)(\mu_c^i - \mu^i)^T, \tag{21}$$

where μ_c^i is the mean of class c of i-th view, μ^i is the overall mean of all classes under i-th view, and n_c^i are the samples of class c for i-th view. In the objective function of (20), the first part arises from the idea of classical Linear Discriminant Analysis (LDA) in order to exploit discriminant vectors in each view [49]. The positive term α is to make a balance among the objectives, and hence usually set to 1 so that the joint objective will be unbiased towards optimizing $\boldsymbol{w}_i$. In order to balance the relative significance between the CCA part and the LDA part in (20), a tunable parameter $\beta_{i,j}$ is introduced, where $\beta_{i,j} > 0$. Since all the constraints in (13) are nonlinear and the current form has no closed form solution, the constraints are coupled with γ = trace ratio, in order to simplify the problem with a relaxed version using a single constraint.

From (20), it is seen that the class label information within each view are considered in GMA, which makes it discriminative for multiple view recognition [50]. However, only the discriminant information within each individual view are employed in GMA while the discriminant information from the inter-view are left unconsidered, which may degrade the performance of inter-view matching. As discussed in section III-C, DCCA in [44] proposes an effective supervised feature extraction method for CCA, by exploiting discriminant information between views. From (11) it is seen that DCCA and CCA has similar optimization objectives [51]. In order to effectively make full use of correlation information within each view and between different views, this work proposes to combine intra-view and inter-view discriminant correlation analysis, and therefore designs the following Generalized Inter-view and Intra-view Discriminat Correlation Analysis (GI^{2}DCA), which preserves both interview and intraview class structures as follows:

$$\max_{\boldsymbol{w}_1,\dots,\boldsymbol{w}_N} \sum_{i}^{M} \alpha_i \boldsymbol{w}_i^T \boldsymbol{S}_i \boldsymbol{w}_i + \sum_{\substack{i,j=1 \\ i\neq j}}^{M} \beta_{i,j} \boldsymbol{w}_i^T \boldsymbol{X}_i \boldsymbol{G} \boldsymbol{X}_j^T \boldsymbol{w}_j$$
$$\text{s.t. } \sum_{i}^{M} \gamma_i \boldsymbol{w}_i^T \boldsymbol{X}_i \boldsymbol{X}_i^T \boldsymbol{w}_i = 1, \tag{22}$$

where $\boldsymbol{G}$ is formulated according to (10). In GI^{2}DCA, samples from different views are projected into a discriminant common space by using M transforms, one for each view. In this common space, samples in one class from multiple views are close to each other, while samples in different classes from multiple views are far away from each other. Therefore, both inter-view and intra-view class structures are preserved. Applying Lagrange multiplier on (22),

the optimization problem of GI^{2}DCA can be solved by a generalized eigenvalue problem following the similar approach of MCCA:

$$\boldsymbol{T}\boldsymbol{w} = \lambda\hat{\boldsymbol{D}}\boldsymbol{w}, \tag{23}$$

where $\boldsymbol{T}$ and $\hat{\boldsymbol{D}}$ are defined as follows, respectively:

$$\boldsymbol{T} = \begin{bmatrix} \alpha_1\boldsymbol{S}_1 & \dots & \beta_{1,N}\boldsymbol{X}_1\boldsymbol{G}\boldsymbol{X}_N^T \\ \vdots & \ddots & \vdots \\ \beta_{N,1}\boldsymbol{X}_N\boldsymbol{G}\boldsymbol{X}_1^T & \dots & \alpha_N\boldsymbol{S}_N \end{bmatrix}. \tag{24}$$

$$\hat{\boldsymbol{D}} = \begin{bmatrix} \gamma_1\boldsymbol{X}_1\boldsymbol{X}_1^T & \dots & \boldsymbol{0} \\ \vdots & \ddots & \vdots \\ \boldsymbol{0} & \dots & \gamma_M\boldsymbol{X}_M\boldsymbol{X}_M^T \end{bmatrix}. \tag{25}$$

The number of non-negative eigenvalues for the general eigenvalue decomposition in Eq. (23) is $r \leq min(d_1, ..., d_M)$, with the assumption that all $\boldsymbol{X}_i$ are of full rank. It can be noted that, this GI^{2}DCA scheme requires finding the eigenvectors of matrices with $d_i \times d_i$ dimensionalities. Defining $d := max_i d_i$, it can be checked that GI^{2}DCA incurs complexity of order $O(d^3M)$. Once the linear transforms $\boldsymbol{w}_i|_{i=1}^{M}$ are obtained through the above approach, the transformed features, $\boldsymbol{Z_i}$ are calculated by projecting $\boldsymbol{X}_i$ on the calculated $\boldsymbol{w}_i$ as,

$$\boldsymbol{Z}_i = \boldsymbol{w}_i^T\boldsymbol{X}_i, \tag{26}$$

where $\boldsymbol{Z}_i \in \mathbb{R}^{r\times n}$ and $i = 1, 2, \dots, M$. Finally, the average canonical variate of the M datasets is calculated as,

$$\boldsymbol{Z} = \frac{1}{M}\sum_{i=1}^{M}\boldsymbol{Z}_i. \tag{27}$$

$\boldsymbol{Z}$ in (27) represents the most common features that are shared among M sets of training data.

As described in section IV-A.1, in the proposed MuDLoc system, the CSI amplitude and phase feature images collected from M APs (views) are denoted by $\boldsymbol{X_i} \in \mathbb{R}^{d_{X_i}\times n}$ and $\boldsymbol{Y_i} \in \mathbb{R}^{d_{Y_i}\times n}$, respectively. GI^{2}DCA is implemented to find multiple linear transforms (i.e. spatial filters) $\boldsymbol{w}_{X_1}$,$\boldsymbol{w}_{X_2}$,...,$\boldsymbol{w}_{X_N}$ that result in the maximization of overall correlation among the canonical variates $\boldsymbol{Z}_{X_1}$,$\boldsymbol{Z}_{X_2}$,...,$\boldsymbol{Z}_{X_N}$ obtained using (26). The transformed amplitude feature from M views, $\boldsymbol{Z}_X \in \mathbb{R}^{r_X\times n}$ is then calculated using (27). In a similar approach, the transformed phase feature from M views are calculated as $\boldsymbol{Z}_Y \in \mathbb{R}^{r_Y\times n}$. Finally, these amplitude and phase difference features extracted from multi-view CSI Data are stacked to obtain the single unified discriminant feature set, $\boldsymbol{Z}$ as follows:

$$\boldsymbol{Z} = \begin{pmatrix} \boldsymbol{Z}_X \\ \boldsymbol{Z}_Y \end{pmatrix}. \tag{28}$$

$\boldsymbol{Z}$ is called the Multi-view Discriminant Feature Image (MDFI) of CSI. MDFI is more discriminative than any of the input feature image. GI^{2}DCA not only finds effective discriminant information over the multiple views of data but also eliminates redundant information within the features of each view, thereby improves the localization performance.

B. ONLINE PHASE

After the aforementioned calibration procedure of training feature optimization in the offline phase, the linear transformations for the amplitude feature, $\hat{\boldsymbol{x}}_i$ of test location t are calculated as,

$$\boldsymbol{Z}_{\hat{\boldsymbol{x}}_i} = \boldsymbol{w}_{\boldsymbol{X}_i}{}^T\hat{\boldsymbol{x}}_i, i = 1, 2, \dots, M. \tag{29}$$

Similarly, the linear transformations for the phase feature, $\hat{y}_i$ of test location, t are calculated as,

$$\boldsymbol{Z}_{\hat{y}_i} = \boldsymbol{w}_{\boldsymbol{Y}_i}{}^T\hat{\boldsymbol{y}}_i. \tag{30}$$

The average canonical variate, $\boldsymbol{Z}_{\hat{\boldsymbol{x}}}$ and $\boldsymbol{Z}_{\hat{\boldsymbol{y}}}$ for test location t are then calculated using (27). Finally the MDFI for test location t is calculated as,

$$\boldsymbol{Z}_{test,t} = \begin{pmatrix} \boldsymbol{Z}_{\hat{\boldsymbol{x}}} \\ \boldsymbol{Z}_{\hat{\boldsymbol{y}}} \end{pmatrix} \tag{31}$$

Finally, the test location's cell Id is recognized using the simple but efficient Euclidean Distance (ED) based similarity measure as following,

$$\underset{c}{\text{argmin}}\ \|\boldsymbol{Z}_{test,t} - \boldsymbol{Z}_{train,c}\|_2, \tag{32}$$

where, $c \in [1, 2, \dots, C]$. The overall system architecture for MuDLoc system is shown in Fig. 3.

V. EXPERIMENTAL STUDY

A. EXPERIMENTAL CONFIGURATION

The proposed MuDLoc system consists of three basic hardware elements in a WLAN infrastructure: access points (AP), detecting points (DP) and a server. A radio frequency (RF) link is established for each pair of AP and DP. In order to measure CSI data in 5 GHz band, the system uses Lenovo laptops as the access points (AP) and a desktop computer as the detection point (DP). Both devices are equipped with an Intel 5300 Network Interface Card (NIC). The operating system is Ubuntu desktop 14.04 LTS OS. The transmitter or access points are set in the injection mode. The receiver or DP is set in the monitor mode. Then 5 GHZ CSI data are obtained by using the packet injection technique based on LORCON version 1 from the receiver NIC. The APs periodically broadcast beacon messages. Once the beacon message is received, the raw PHY layer CSIs across multiple subcarriers from the multiple APs (views) are recorded by the DP and sent to the server in order to store and process.[1] Finally the localization is performed by the server through multi-view discriminant learning approach. We use a host PC (Intel i7-4790CPU 3.60 GHz, 8GB RAM), that serves as the centralized server for location estimation. Using the Linux 802.11n tool [12], [13], for each AP, the DP collects CSI data for 30 subcarriers for each Tx-Rx antenna pair. Therefore, 3×3 Tx-Rx antenna pairs for each AP-DP link is utilized. Finally, the amplitude and phase data are extracted for the training and test stages as described in Section IV-A.1

[1] sample data used in the experiment can be found here: https://github.com/tfsanam/MuDLoc/tree/exp1

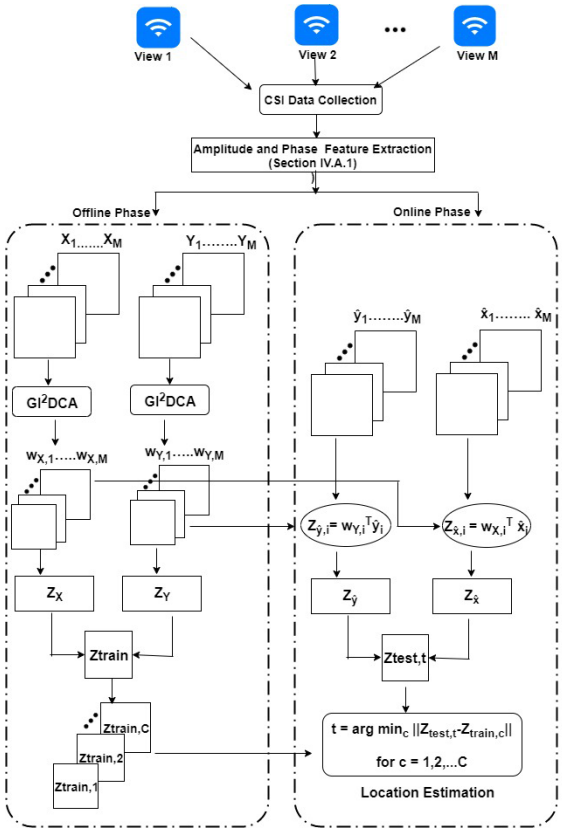

FIGURE 3. MuDLoc system architecture.

in order to implement MuDLoc with GI^{2}DCA approach. The performance of MuDLoc is verified in various scenarios and the resulting location errors in different environments are compared with several benchmark schemes. It is found from the experimental results that in an open indoor space, where there are fewer or no obstacles in the area of interest, the performance of indoor localization is better than that in a complex environment where there are fewer LOS paths. The experimental results are presented from two typical indoor localization environments, as described in the following.

1) RESEARCH LABORATORY

This is a research laboratory with an area of 6 $m \times 5$ m in the CoRE Building of Rutgers University. Fig. 4 shows the testbed layout of MuDLoc in the research laboratory. The lab represents a cluttered environment, equipped with office desks, shelfs, desktops, chairs etc., which block most of the LOS paths and form a complex radio propagation environment. The area is virtually partitioned into 20 uniform square grids/cells, each of which is $0.50m \times 0.50m$ in size. 3 different APs are placed in 3 different random places in order to exploit the multi-view approach.

2) CORRIDOR

This is a long corridor at fifth floor of CoRE Building of Rutgers University with dimension 2 $m \times 10$ m. The corridor we choose is almost empty; therefore, most of the measured

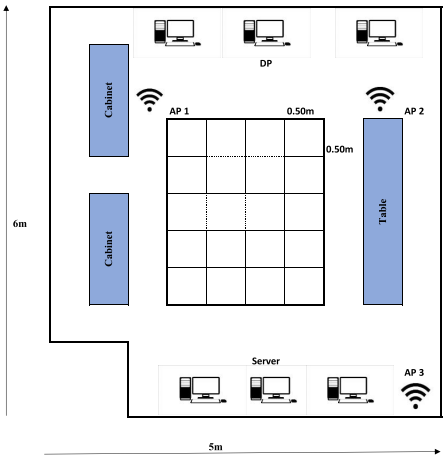

FIGURE 4. The layout of the testbed in a research laboratory.

locations have LOS receptions. As in Fig. 5, we place 3 APs at different random locations on the floor to measure CSI data. 20 positions are chosen uniformly scattered with half-meter spacing along a straight line for the corridor experiments.

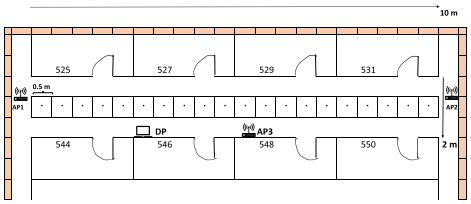

FIGURE 5. The layout of the testbed in a corridor.

All experiments are conducted during weekdays. For each location, we get 3000 samples for each of the APs (views). These time domain samples collected for each of the APs are grouped in order to create feature images for each location. The entire dataset is partitioned into training sets, validation sets and test sets using a ratio of 6:2:2. Following the suggestions in [33], μ is set to 1, γ is set as trace ratio, and 5-fold cross validation are used to select tuning parameter β among [0, 1000]. Time consumption of the training and the online localization stage are 2.74 s and 1.68 s, respectively. Four representative schemes are built from the literature, i.e., PC-DfL [8], Pilot [19], Pairwise CCA (PWCCA) [28] and MCCA [30], which are discussed in Section I. In order to ensure a fair comparison, same dataset obtained for the 5 GHz band is used by all the schemes. Extensive experiments with the schemes are conducted in the above two representative indoor environments to evaluate the performance of the proposed method.

B. LOCALIZATION PERFORMANCE

First the performance of MuDLoc system with proposed GI^{2}DCA approach is evaluated in terms of mean distance error and standard deviation; and are compared with the RSS-based localization approach PC-DfL [8] and CSI-based approach Pilot [19]. The proposed system is also compared

with related existing multi-data processing methods including pairwise CCA (PWCCA) [28] and MCCA [30], when applied for indoor localization. Among them, PWCCA, is a two-view method; therefore, the pairwise strategy for multi-view classification is exploited for comparison. The results are presented for laboratory and corridor scenarios in Table 1 and 2, respectively. For the laboratory scenario, where there exists abundant multipath and shadowing effect, the mean error of MuDLoc is 0.2449 m and the STD error is 0.4449 m, as shown in Table 1. In the corridor environment, where there exists more LOS receptions, the mean error of MuDLoc is 0.15 m and the STD error is 0.3095 m, as shown in Table 2. MuDLoc outperforms the other multi-view learning approach, PWCCA and MCCA in both scenarios. MuDLoc achieves a 65% improvement over MCCA by exploiting a inter-view and intra-view discriminnat learning approach in multi-view analysis. Moreover, all the CSI based schemes outperforms the RSS based approach, i.e., PC-DfL. The latter has a mean error of 1.3 m in the laboratory scenario and 1.16 m in the corridor scenario.

TABLE 1. Comparison of mean distance error and standard deviation for different schemes in the laboratory environment.

Algorithms	Mean distance error (m)	Std. dev. (m)
PC-DfL	1.3000	0.8346
Pilot	1.01667	0.8242
PWCCA	0.8665	0.7922
MCCA	0.7032	0.4919
MuDLoc (GI^{2}DCA)	0.2449	0.4449

TABLE 2. Comparison of mean distance error and standard deviation for different schemes in the corridor environment.

Algorithms	Mean distance error (m)	Std. dev. (m)
PC-DfL	1.1589	0.6469
Pilot	1.1349	0.6581
PWCCA	0.7192	0.7718
MCCA	0.6888	0.6040
MuDLoc(GI^{2}DCA)	0.1500	0.3095

Fig. 6 presents the CDF of distance errors for different methods in the laboratory environment. MuDLoc has 65% of the test locations having an error less than or equal to 0.5 m, while that for the other methods is 42% or less. We also find that approximately 90% of the test locations for MuDLoc have an error under 1 m, while the percentage of test locations having a smaller error than 1 m are 75%, 68%, 37% and 33% for MCCA, PWCCA, Pilot and PC-DfL, respectively. Thus, MuDLoc achieves the best performance in terms of distance error in this experiment.

In Fig. 7, the CDF of distance errors for different methods in the corridor environment are presented. With MuDLoc, 78% of the test positions have an error smaller than 0.5mm, while with MCCA, PWCCA, Pilot and PC-DfL, close to 27%, 48%, 5% and 10% of the test positions, respectively, have an error smaller than 0.5 m. Results also show that approximately 95% of the test locations for MuDLoc have an error under 1 m, while that for the other methods is 67%

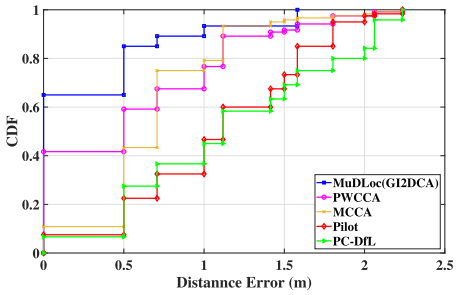

FIGURE 6. CDF of distance error for laboratory scenario.

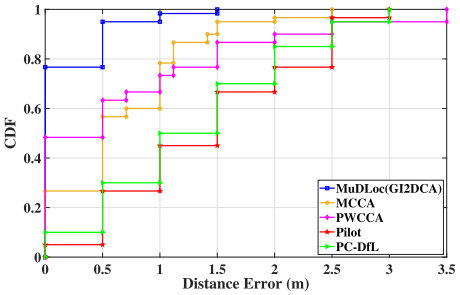

FIGURE 7. CDF of distance error for corridor scenario.

or less. Thus, MuDLoc also achieves the best performance for corridor environment. This is because the other methods are either designed to work with single AP or consider the average value for multiple APs. Morover, all other methods use only the amplitude feature of CSI or RSS value for localization, while MuDLoc exploits CSIs from multiple APs through multiview discriminant analysis and fuses transformed amplitude and phase-based features of CSI into a single feature, which is more discriminative than the individual ones. This feature fusion method reduces the redundant information between two input features, and therefore will be more effective for better localization.

C. IMPACT OF USING AMPLITUDE AND PHASE DIFFERENCE FEATURES OF CSI

The proposed MuDLoc system utilizes CSI as observation measurements for indoor localization, which provides amplitude and phase information. The contribution of these amplitude and phase features of CSI data are analyzed through the evaluation of the system performance when using amplitude information, phase information, and both the amplitude and phase information of CSI. Fig. 8 reveals that The performance for corridor scenario is always better than the laboratory scenario in all the cases due to more LOS reception for most of the measured positions. However, the MuDLoc system with GI^{2}DCA approach could achieve reasonable localization accuracy for both indoor scenarios even using only one type of measurement (either amplitude or phase). The mean distance error can be further decreased to as low as 0.25 m for laboratory scenario and 0.15 m for corridor scenario if using both the amplitude and phase measurements. Thus, utilizing the amplitude and phase difference features of CSI in terms of amplitude and phase information from MIMO OFDM system

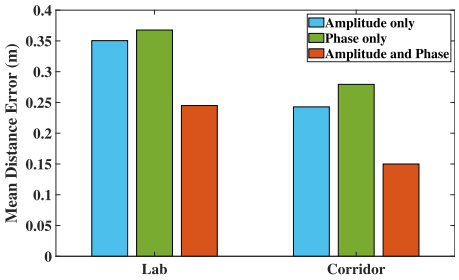

FIGURE 8. Mean distance error for different modality of CSI measurements.

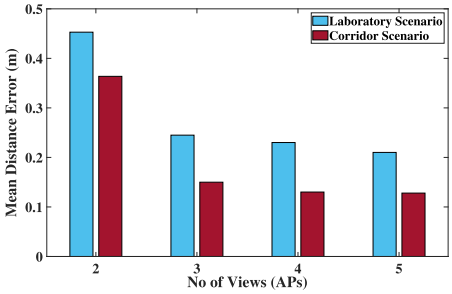

FIGURE 9. Mean distance error in laboratory for different no of views (APS).

facilitates to improve the localization performance to a great extent.

D. IMPACT OF THE NUMBER OF SAMPLES IN THE ONLINE TEST

The effect of the number of packets used in the online test phase of MuDLoc are also evaluated in the study. In the experiments, the location of the target is estimated using different numbers of packets for the two indoor environments. The experiments are performed using 100, 200, 300, 400, and 500 packets in the online test for location estimation. In Table 3, the mean distance errors for different numbers of packets in the laboratory and corridor experiments are shown. Results show that the mean distance error in the corridor experiment is lower than that in the laboratory experiment for different amounts of packets. Moreover, with the increase of packets, the mean distance error for both experiments is decreased. It can be noted that the maximum distance errors for the laboratory and corridor experiments are 0.458 m and 0.391 m, respectively, while the minimum distance errors for the laboratory and corridor experiments are 0.205 m and 0.109 m, respectively. Intuitively, with very low number of packets, we do not have sufficient samples to localize a target with better precision, while larger number of samples enables us to have sufficient data to localize a target more precisely. However, the processing time increases with the increase in number of samples. Therefore, MuDLoc chooses 300 packets in online test for all experiments, with which the system can obtain a satisfactory localization performance with a lower computational complexity.

TABLE 3. Mean distance error versus the number of packets used in online test phase.

# of packets	100	200	300	400	500
Laboratory	0.45 m	0.28 m	0.24 m	0.23 m	0.20 m
Corridor	0.39 m	0.23 m	0.15 m	0.12 m	0.10 m

E. IMPACT OF THE NUMBER OF VIEWS (APs)

Finally, the impact of the number of views (APs) on localization performance is evaluated for the proposed method in the two indoor environments. The experiments are conducted with multiple views (APs) to evaluate the performance of the proposed system. Fig. 9 presents the performance of MuDLoc (GI^{2}DCA) system in terms of the mean distance errors for different number of APs in laboratory and corridor environments. However the results for one AP is not included, since with one AP, multi-view strategy does not work (which requires two or more APs), and therefore we are unable to extract the inter-view discriminant features of CSIs while considering only one AP. It is noticed that, with the increase in number of views/APs, the mean error is decreased for both indoor deployments. This is because, the more the number of APS, the richer the multipath information that can be obtained to estimate the location. However, results show that, for both environments, the decrease in mean distance error are relatively small when the number of AP is increased to 4 or more. Since MuDLoc can obtain fairly low localization errors using only 3 APs for both indoor deployments, this work considers using 3 AP for exploiting the multi-view approach in order to achieve the higher localization accuracy with lower deployment cost.

Although the MuDLoc scheme with three or more AP achieves lower mean distance errors, it takes more time for processing the CSI values from multiple AP as input data for each packet. We evaluate the average processing time to estimate the target position in the test phase using 300 received packets. The processing time is measured as the CPU occupation time for the MATLAB R2016a program running on the centralized server. Results in Table 4 show that, in the laboratory scenario, the single-view scheme (i.e. Pilot) takes 1.89 s, on average, to estimate the target position, whereas the multi-view scheme (MuDLoc) takes around 2.18 s, 2.35 s, 2.73 s and 3.09 s for processing CSI values from 2, 3, 4, and 5 APs, respectively, as input data to estimate the location. Therefore, with the increase in no of views (APs), the execution time increases. As shown in Fig. 9, MuDLoc can obtain fairly low localization errors using only 3 APs for laboratory scenario and the mean processing time is 2.35 s, which is lower than that for 4 AP or 5 AP systems. Moreover, the difference in execution time is small when compared with single view approach, although the multi-view approach processes

TABLE 4. Comparison of mean processing time for single-view vs, multi-view scheme in the laboratory environment.

No. of views	single-view	multi-view (MuDLoc)			
	Pilot	2 AP	3 AP	4 AP	5 AP
Proc. time (s)	1.89	2.18	2.35	2.73	3.09

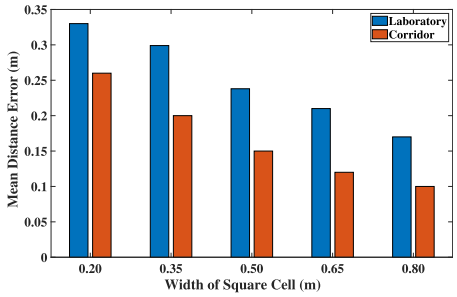

FIGURE 10. Mean distance error versus cell width of square grid.

three times input data than that in the single view (single-AP) scheme. The three-view MuDLoc takes about 29% extra processing time than single-view approach, but it can achieve a 83% improvement in localization precision for laboratory environment and the latter is generally more important for indoor localization.

F. IMPACT OF CELL RESOLUTION

The performance of localization varies with the cell resolution. It is intuitive that with the increase in cell resolution the accuracy increases and vice versa. We conducted several experiments by varying cell resolution and chose 0.5 m $\times$ 0.5 m as our cell size for this experiment. The impact of cell resolution on the mean distance error for research laboratory and corridor are presented in Fig. 10. As we can see, the mean distance error decreases if the cell width of the square cell is increased from 0.5 m to 0.65 m or more. On the other hand, if we decrease the cell width from 0.5 m to 0.35 m or less, the error increases. However, assuming that the target is located at the center of a cell, we achieved mean distance error of 0.24 m and 0.15 m when the cell width is 0.50 m for laboratory and corridor experiments, respectively. These results indicate that the target is localized within the cell with mean distance error of 0.24 m and 0.15 m from the center of the cell for the above experimental scenarios. When the cell resolution is decreased, the mean distance error increases to more than half of the cell width. Therefore, in this experiment we chose 0.5 m $\times$ 0.5 m as our cell size for both experiment scenarios.

VI. CONCLUSION

This paper presents MuDLoc, a multi-view discriminant learning approach for indoor localization that exploits both the amplitude and the phase information of CSI in MIMO OFDM systems. In MuDLoc, CSI information for all the subcarriers from 3 $\times$ 3 MIMO channels are collected from multiple APs and analyzed with a multi-view learning approach to extract joint spatial features. In order to take discriminant information across multiple cells/locations and multiple views into account, the proposed MuDLoc system implements GI^{2}DCA, which preserves both inter-view and intra-view class structures through a discriminant correlation analysis. Both amplitude and phase information are utilized in order to exploit the complete multipath information from CSI measurements. These discriminant features extracted from the GI^{2}DCA are used for effective, high accuracy device free indoor localization by transforming the localization problem into a cell classification problem using pattern matching. The proposed MuDLoc scheme was validated in two representative indoor environments and was found to outperform several existing RSS and CSI based localization schemes. The effect of different modalities of CSI data as well as system parameters on MuDLoc performance are examined. It was found that MuDLoc can achieve good performance with lower localization error under such scenarios.

REFERENCES

[1] H. Liu, H. Darabi, P. Banerjee, and J. Liu, "Survey of wireless indoor positioning techniques and systems," *IEEE Trans. Syst., Man, Cybern. C, Appl. Rev.*, vol. 37, no. 6, pp. 1067–1080, Nov. 2007.
[2] A. Yassin, Y. Nasser, M. Awad, A. Al-Dubai, R. Liu, C. Yuen, R. Raulefs, and E. Aboutanios, "Recent advances in indoor localization: A survey on theoretical approaches and applications," *IEEE Commun. Surveys Tuts.*, vol. 19, no. 2, pp. 1327–1346, 2nd Quart., 2017.
[3] Z. Yang, Z. Zhou, and Y. Liu, "From RSSI to CSI: Indoor localization via channel response," *ACM Comput. Surv.*, vol. 46, no. 2, Dec. 2013, Art. no. 25, doi: 10.1145/2543581.2543592.
[4] S. He and S.-H.-G. Chan, "Wi-Fi fingerprint-based indoor positioning: Recent advances and comparisons," *IEEE Commun. Surveys Tuts.*, vol. 18, no. 1, pp. 466–490, 1st Quart., 2016.
[5] P. Bahl and V. Padmanabhan, "RADAR: An in-building RF-based user location and tracking system," in *Proc. IEEE Conf. Comput. Communications (INFOCOM), 19th Annu. Joint Conf. IEEE Comput. Commun. Societies*, vol. 2, Nov. 2002, pp. 775–784,.
[6] M. Youssef and A. Agrawala, "The Horus WLAN location determination system," in *Proc. 3rd Int. Conf. Mobile Syst., Appl., Services (MobiSys)*. New York, NY, USA: ACM, 2005, pp. 205–218, doi: 10.1145/1067170.1067193.
[7] S. Sadowski and P. Spachos, "RSSI-based indoor localization with the Internet of Things," *IEEE Access*, vol. 6, pp. 30149–30161, 2018.
[8] C. Xu, B. Firner, Y. Zhang, and R. E. Howard, "The case for efficient and robust RF-based device-free localization," *IEEE Trans. Mobile Comput.*, vol. 15, no. 9, pp. 2362–2375, Sep. 2016.
[9] D. Konings, F. Alam, F. Noble, and E. M.-K. Lai, "SpringLoc: A device-free localization technique for indoor positioning and tracking using adaptive RSSI spring relaxation," *IEEE Access*, vol. 7, pp. 56960–56973, 2019.
[10] Z. Wang, K. Jiang, Y. Hou, Z. Huang, W. Dou, C. Zhang, and Y. Guo, "A survey on CSI-based human behavior recognition in through-the-wall scenario," *IEEE Access*, vol. 7, pp. 78772–78793, 2019.
[11] B. Tan, Q. Chen, K. Chetty, K. Woodbridge, W. Li, and R. Piechocki, "Exploiting WiFi channel state information for residential healthcare informatics," *IEEE Commun. Mag.*, vol. 56, no. 5, pp. 130–137, May 2018.
[12] D. Halperin, W. Hu, A. Sheth, and D. Wetherall, "Predictable 802.11 packet delivery from wireless channel measurements," in *Proc. Conf. (ACM SIGCOMM)*. New York, NY, USA: ACM, 2010, pp. 159–170, doi: 10.1145/1851275.1851203.
[13] D. Halperin, W. Hu, A. Sheth, and D. Wetherall, "Tool release: Gathering 802.11n traces with channel state information," *SIGCOMM Comput. Commun. Rev.*, vol. 41, no. 1, p. 53, Jan. 2011, doi: 10.1145/1925861.1925870.
[14] K. Wu, J. Xiao, Y. Yi, M. Gao, and L. M. Ni, "FILA: Fine-grained indoor localization," in *Proc. IEEE INFOCOM*, Mar. 2012, pp. 2210–2218.
[15] X. Wang, L. Gao, and S. Mao, "BiLoc: Bi-modal deep learning for indoor localization with commodity 5 GHz WiFi," *IEEE Access*, vol. 5, pp. 4209–4220, 2017.
[16] Y. Chapre, A. Ignjatovic, A. Seneviratne, and S. Jha, "CSI-MIMO: Indoor Wi-Fi fingerprinting system," in *Proc. 39th Annu. IEEE Conf. Local Comput. Netw.*, Sep. 2014, pp. 202–209.
[17] H. Chen, Y. Zhang, W. Li, X. Tao, and P. Zhang, "ConFi: Convolutional neural networks based indoor Wi-Fi localization using channel state information," *IEEE Access*, vol. 5, pp. 18066–18074, 2017.
[18] T. F. Sanam and H. Godrich, "An improved CSI based device free indoor localization using machine learning based classification approach," in *Proc. 26th Eur. Signal Process. Conf. (EUSIPCO)*, Sep. 2018, pp. 2390–2394.

[19] J. Xiao, K. Wu, Y. Yi, L. Wang, and L. M. Ni, "Pilot: Passive device-free indoor localization using channel state information," in *Proc. IEEE 33rd Int. Conf. Distrib. Comput. Syst.*, Jul. 2013, pp. 236–245.
[20] J. Wang, J. Xiong, H. Jiang, K. Jamieson, X. Chen, D. Fang, and C. Wang, "Low human-effort, device-free localization with fine-grained subcarrier information," *IEEE Trans. Mobile Comput.*, vol. 17, no. 11, pp. 2550–2563, Nov. 2018.
[21] T. F. Sanam and H. Godrich, "Device free indoor localization using discriminant features of CSI a canonical correlation paradigm," in *Proc. 52nd Asilomar Conf. Signals, Syst., Comput.*, Oct. 2018, pp. 423–427.
[22] L. Zhang, Q. Gao, X. Ma, J. Wang, T. Yang, and H. Wang, "DeFi: Robust training-free device-free wireless localization with WiFi," *IEEE Trans. Veh. Technol.*, vol. 67, no. 9, pp. 8822–8831, Sep. 2018.
[23] S. Savazzi, S. Sigg, M. Nicoli, V. Rampa, S. Kianoush, and U. Spagnolini, "Device-free radio vision for assisted living: Leveraging wireless channel quality information for human sensing," *IEEE Signal Process. Mag.*, vol. 33, no. 2, pp. 45–58, Mar. 2016.
[24] T. Xin, B. Guo, Z. Wang, P. Wang, J. C. K. Lam, V. Li, and Z. Yu, "FreeSense: A robust approach for indoor human detection using Wi-Fi signals," in *Proc. ACM Interact. Mob. Wearable Ubiquitous Technol.*, Sep. 2018, vol. 2, no. 3, Art. no. 143, doi: 10.1145/3264953.
[25] X.-Y. Jing, F. Wu, X. Dong, S. Shan, and S. Chen, "Semi-supervised multi-view correlation feature learning with application to Webpage classification," in *Proc. AAAI*, 2017, pp. 1–8.
[26] F. Wu, X.-Y. Jing, J. Zhou, Y. Ji, C. Lan, Q. Huang, and R. Wang, "Semi-supervised multi-view individual and sharable feature learning for Webpage classification," in *Proc. World Wide Web Conf. (WWW)*. New York, NY, USA: ACM, 2019, pp. 3349–3355, doi: 10.1145/3308558.3313492.
[27] F. Wu, X.-Y. Jing, and D. Yue, "Multi-view discriminant dictionary learning via learning view-specific and shared structured dictionaries for image classification," *Neural Process. Lett.*, vol. 45, no. 2, pp. 649–666, Apr. 2017, doi: 10.1007/s11063-016-9545-7.
[28] H. Hotelling, "Relations between two sets of variates," *Biometrika*, vol. 28, no. 3/4, pp. 321–327, Dec. 1936.
[29] M. Haghighat, M. Abdel-Mottaleb, and W. Alhalabi, "Discriminant correlation analysis: Real-time feature level fusion for multimodal biometric recognition," *IEEE Trans. Inf. Forensics Security*, vol. 11, no. 9, pp. 1984–1996, Sep. 2016.
[30] J. Rupnik and J. Shawe-Taylor, "Multi-view canonical correlation analysis," in *Proc. SiKDD*, Jan. 2010.
[31] A. Nielsen, "Multiset canonical correlations analysis and multispectral, truly multitemporal remote sensing data," *IEEE Trans. Image Process.*, vol. 11, no. 3, pp. 293–305, Mar. 2002.
[32] J. R. Kettenring, "Canonical analysis of several sets of variables," *Biometrika*, vol. 58, no. 3, pp. 433–451, 1971, doi: 10.1093/biomet/58.3.433.
[33] A. Sharma, A. Kumar, H. Daume, D. W. Jacobs "Generalized multiview analysis: A discriminative latent space," in *Proc. IEEE Conf. Comput. Vis. Pattern Recognit. (CVPR)*. Washington, DC, USA: IEEE Computer Society, Jun. 2012, pp. 2160–2167. [Online]. Available: http://dl.acm.org/citation.cfm?id=2354409.2355114
[34] X.-Y. Jing, R.-M. Hu, Y.-P. Zhu, S.-S. Wu, C. Liang, and J.-Y. Yang, "Intra-view and inter-view supervised correlation analysis for multi-view feature learning," in *Proc. 28th AAAI Conf. Artif. Intell. (AAAI)*. AAAI Press, 2014, pp. 1882–1889.
[35] T. F. Sanam and H. Godrich, "FuseLoc: A CCA based information fusion for indoor localization using CSI phase and amplitude of Wifi signals," in *Proc. IEEE Int. Conf. Acoust., Speech Signal Process. (ICASSP)*, May 2019, pp. 7565–7569.
[36] J. Gjengset, J. Xiong, G. McPhillips, and K. Jamieson, "Phaser: Enabling phased array signal processing on commodity WiFi access points," in *Proc. 20th Annu. Int. Conf. Mobile Comput. Netw. (MobiCom)*. New York, NY, USA: ACM, 2014, pp. 153–164, doi: 10.1145/2639108.2639139.
[37] H. Zhu, Y. Zhuo, Q. Liu, and S. Chang, "Π-splicer: Perceiving accurate CSI phases with commodity WiFi devices," *IEEE Trans. Mobile Comput.*, vol. 17, no. 9, pp. 2155–2165, Sep. 2018.
[38] M. B. Akbar, D. G. Taylor, and G. D. Durgin, "Amplitude and phase difference estimation bounds for multisensor based tracking of RFID Tags," in *Proc. IEEE Int. Conf. RFID (RFID)*, Apr. 2015, pp. 105–112.
[39] X. Wang, L. Gao, and S. Mao, "CSI phase fingerprinting for indoor localization with a deep learning approach," *IEEE Internet Things J.*, vol. 3, no. 6, pp. 1113–1123, Dec. 2016.
[40] C. Wu, Z. Yang, Z. Zhou, K. Qian, Y. Liu, and M. Liu, "PhaseU: Real-time LOS identification with WiFi," in *Proc. IEEE Conf. Comput. Commun. (INFOCOM)*, Apr. 2015, pp. 2038–2046.
[41] Y. Xie, Z. Li, and M. Li, "Precise power delay profiling with commodity Wi-Fi," in *Proc. 21st Annu. Int. Conf. Mobile Comput. Netw. (MobiCom)*. New York, NY, USA: ACM, 2015, pp. 53–64, doi: 10.1109/TMC.2018.2860991.
[42] M. Speth, S. A. Fechtel, G. Fock, and H. Meyr, "Optimum receiver design for wireless broad-band systems using OFDM. I," *IEEE Trans. Commun.*, vol. 47, no. 11, pp. 1668–1677, Nov. 1999.
[43] M. Borga, "Canonical correlation: A tutorial," Tech. Rep., 1999.
[44] T. Sun, S. Chen, J. Yang, and P. Shi, "A novel method of combined feature extraction for recognition," in *Proc. 8th IEEE Int. Conf. Data Mining*, Dec. 2008, pp. 1043–1048.
[45] Q.-S. Sun, S.-G. Zeng, Y. Liu, P.-A. Heng, and D.-S. Xia, "A new method of feature fusion and its application in image recognition," *Pattern Recognit.*, vol. 38, no. 12, pp. 2437–2448, Dec. 2005.
[46] Y.-O. Li, T. Adali, W. Wang, and V. Calhoun, "Joint blind source separation by multiset canonical correlation analysis," *IEEE Trans. Signal Process.*, vol. 57, no. 10, pp. 3918–3929, Oct. 2009.
[47] A. Nielsen, "Multiset canonical correlations analysis and multispectral, truly multitemporal remote sensing data," *IEEE Trans. Image Process.*, vol. 11, no. 3, pp. 293–305, Mar. 2002.
[48] O. Ledoit and M. Wolf, "A well-conditioned estimator for large-dimensional covariance matrices," *J. Multivariate Anal.*, vol. 88, no. 2, pp. 365–411, Feb. 2004.
[49] P. N. Belhumeur, J. P. Hespanha, and D. J. Kriegman, "Eigenfaces vs. Fisherfaces: Recognition using class specific linear projection," *IEEE Trans. Pattern Anal. Mach. Intell.*, vol. 19, no. 7, pp. 711–720, Jul. 1997.
[50] M. Kan, S. Shan, H. Zhang, S. Lao, and X. Chen, "Multi-view discriminant analysis," *IEEE Trans. Pattern Anal. Mach. Intell.*, vol. 38, no. 1, pp. 188–194, Jan. 2016.
[51] S. Sun, X. Xie, and M. Yang, "Multiview uncorrelated discriminant analysis," *IEEE Trans. Cybern.*, vol. 46, no. 12, pp. 3272–3284, Dec. 2016.

TAHSINA FARAH SANAM (Student Member, IEEE) received the B.Sc. and M.Sc. degrees in electrical and electronic engineering from the Bangladesh University of Engineering and Technology, Dhaka, Bangladesh, in 2009 and 2012, respectively. She is currently pursuing the Ph.D. degree with the Department of Electrical and Computer Engineering, Rutgers University, Piscataway, NJ, USA.

Her research interests include the areas of machine learning, localization and tracking, and speech signal processing. She won the ECE Ph.D. Research Excellence Award, in Fall 2018, and the School of Graduate Studies 2018-2019 Conference Travel Award at Rutgers. She served as the Vice Chair for the Women in Engineering Affinity Group at the IEEE Bangladesh Section from 2010 to 2011. She is currently serving as the President of the Society of Women Engineers Grad Chapter at Rutgers University.

HANA GODRICH (Senior Member, IEEE) received the B.Sc. degree from the Technion - Israel Institute of Technology, Haifa, in 1987, the M.Sc. degree from Ben-Gurion University, Beer-Sheva, Israel, in 1993, and the Ph.D. degree from the New Jersey Institute of Technology (NJIT), Newark, in 2010, all in electrical engineering.

She is currently an Associate Research Professor with the Electrical and Computer Engineering Department, Rutgers University, Piscataway, NJ, USA. From 2010 to 2012, she was a Research Scholar with Princeton University, Princeton. From 1993 to 1995, she was with Scitex Inc. (currently H-P). From 1996 to 2003, she was a Partner and a Consultant with Enetpower Inc., Israel, where she focuses on power systems design for mission-critical facilities. Her research interests include statistical signal processing with application to wireless sensor networks, communication, smart grid, and radar systems.